OPEN ACCESS Freely available online

PLoS one

In Vivo Detection of Amyloid-β Deposits Using Heavy Chain Antibody Fragments in a Transgenic Mouse Model for Alzheimer's Disease

Rob J. A. Nabuurs[1*☯], Kim S. Rutgers[2☯], Mick M. Welling[1], Athanasios Metaxas[3], Maaike E. de Backer[1], Maarten Rotman[2], Brian J. Bacskai[4], Mark A. van Buchem[1], Silvère M. van der Maarel[2], Louise van der Weerd[1,2,5]

1 Department of Radiology, Leiden University Medical Center, Leiden, The Netherlands, **2** Department of Human Genetics, Leiden University Medical Center, Leiden, The Netherlands, **3** Nuclear Medicine and PET Research, Radionuclide Center, Free University Medical Center, Amsterdam, The Netherlands, **4** Department of Neurology, Massachusetts General Hospital and Harvard Medical School, Charlestown, Massachusetts, United States of America, **5** Department of Anatomy and Embryology, Leiden University Medical Center, Leiden, The Netherlands

Abstract

This study investigated the *in vivo* properties of two heavy chain antibody fragments (V_HH), ni3A and pa2H, to differentially detect vascular or parenchymal amyloid-β deposits characteristic for Alzheimer's disease and cerebral amyloid angiopathy. Blood clearance and biodistribution including brain uptake were assessed by bolus injection of radiolabeled V_HH in APP/PS1 mice or wildtype littermates. In addition, *in vivo* specificity for Aβ was examined in more detail with fluorescently labeled V_HH by circumventing the blood-brain barrier via direct application or intracarotid co-injection with mannitol. All V_HH showed rapid renal clearance (10–20 min). Twenty-four hours post-injection ^{99m}Tc-pa2H resulted in a small yet significant higher cerebral uptake in the APP/PS1 animals. No difference in brain uptake were observed for ^{99m}Tc-ni3A or DTPA(^{111}In)-pa2H, which lacked additional peptide tags to investigate further clinical applicability. *In vivo* specificity for Aβ was confirmed for both fluorescently labeled V_HH, where pa2H remained readily detectable for 24 hours or more after injection. Furthermore, both V_HH showed affinity for parenchymal and vascular deposits, this in contrast to human tissue, where ni3A specifically targeted only vascular Aβ. Despite a brain uptake that is as yet too low for *in vivo* imaging, this study provides evidence that V_HH detect Aβ deposits *in vivo*, with high selectivity and favorable *in vivo* characteristics, making them promising tools for further development as diagnostic agents for the distinctive detection of different Aβ deposits.

Citation: Nabuurs RJA, Rutgers KS, Welling MM, Metaxas A, de Backer ME, et al. (2012) *In Vivo* Detection of Amyloid-β Deposits Using Heavy Chain Antibody Fragments in a Transgenic Mouse Model for Alzheimer's Disease. PLoS ONE 7(6): e38284. doi:10.1371/journal.pone.0038284

Editor: Gayle E. Woloschak, Northwestern University Feinberg School of Medicine, United States of America

Received July 12, 2011; **Accepted** May 3, 2012; **Published** June 4, 2012

Funding: Research was supported by: (1) the Center for Translational Molecular Medicine, LeARN, http://www.ctmm.nl; (2) Innovatiegericht OnderzoeksProgramma (IOP)Genomics, IGE05005, http://www.agentschapnl.nl/nl/programmas-regelingen/iop-genomics; (3) the Center for Medical Systems Biology, CMSB2, http://www.cmsb.nl; and (4) The Netherlands Organisation for Scientific Research (NWO) Athena, 700.58.801, http://www.nwo.nl/nwohome.nsf/pages/NWOA_6ZXCX3. The funders had no role in study design, data collection and analysis, decision to publish, or preparation of the manuscript.

Competing Interests: The authors have declared that no competing interests exist.

* E-mail: R.J.A.Nabuurs@LUMC.nl

☯ These authors contributed equally to this work.

Introduction

Besides neurofibrillary tangles, Alzheimer's disease (AD) is characterized by cerebral deposition of β-amyloid (Aβ) in so-called senile or diffuse plaques [1]. Similar vascular deposits of Aβ associated with cerebral amyloid angiopathy (CAA) lead to loss of vessel wall integrity increasing the risk of brain haemorrhages [2]. Present in 30% of the non-demented population over 60 years of age, CAA co-exists in 90% of the AD patients and forms an important complication in the development of immunotherapeutic strategies [3–5]. Although, the exact role of Aβ regarding the underlying pathogeneses remains unsolved, accumulation is believed to start 20–30 years prior to clinical onset [6,7]. Distinctive *in vivo* detection of the different Aβ deposits therefore renders important knowledge regarding early diagnosis and preventive therapy development.

Currently, a gross differentiation can only be made based on the occipital predilection of CAA, while existing PET ligands, like ^{11}C-PiB, target Aβ in its fibrillar amyloid form rather than specific vascular or parenchymal types of Aβ deposits [8].

Previously, we have selected heavy chain antibody fragments with high affinity specific for either CAA or all types of human Aβ deposits [9]. Derived from the Camelid heavy chain antibody repertoire, which completely lack light chains, their single N-terminal domain (V_HH) is fully capable of antigen binding with affinities comparable with those of conventional antibodies [10,11].

Blood-brain barrier (BBB) passage was shown to be favorable in an *in vitro* assay [12]; therefore, this study assessed the *in vivo* characteristics of two distinct Aβ targeting V_HH, ni3A and pa2H, for their potential use to differentially detect AD and CAA. First, pharmacologic behaviour and biodistribution were examined after administration of radiolabeled V_HH into a transgenic AD/CAA

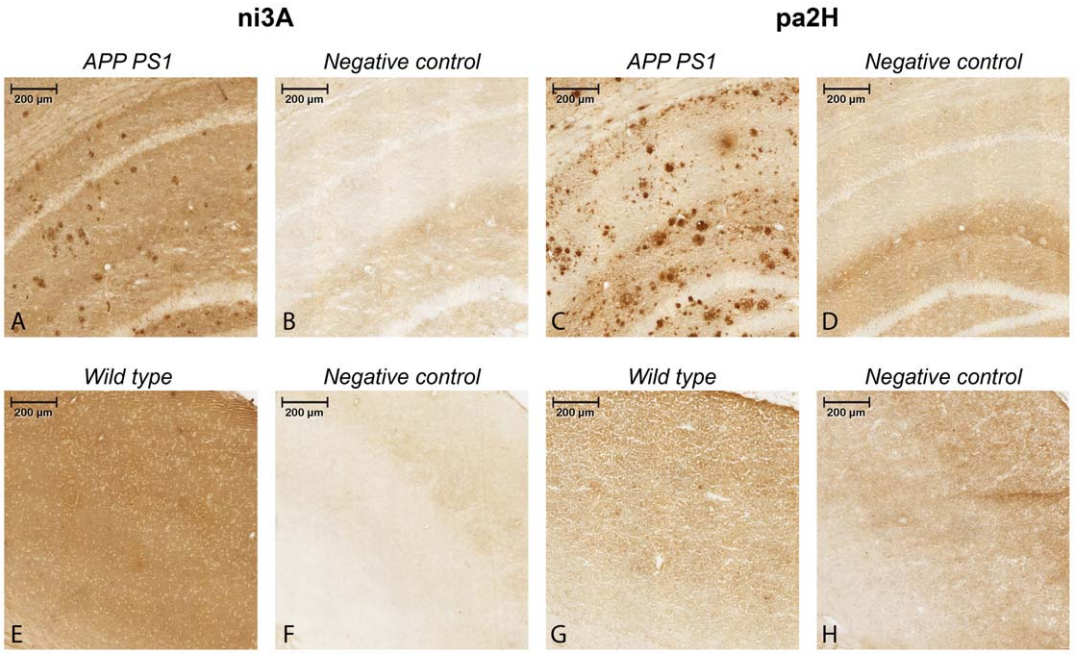

Figure 1. Immunostaining on murine APP/PS1 sections using ni3A and pa2H. The upper panels (**A–D**) show 10× magnifications of the resulting staining with cryosections of aged APP/PS1 mouse brain tissue including negative controls, while the lower panels (**E–H**) show similar staining performed with wildtype littermates.
doi:10.1371/journal.pone.0038284.g001

mouse model. Secondly, fluorescently labeled V_HH were administered after the BBB was circumvented to evaluate their ability to specifically bind Aβ deposits *in vivo*.

Materials and Methods

Production of ni3A and pa2H

V_HH ni3A and pa2H were selected from respectively a non-immune or an immune library created after immunisation with post-mortem brain parenchyma of a patient with Down's syndrome. V_HH were subcloned and produced as previously reported including a myc- or VSV-tag for detection and a *his*-tag for purification [9]. Similarly, pa2H free of any additional peptide tags was commercially produced by overexpression in yeast (BAC, Leiden, the Netherlands).

Animal studies

All studies were performed using 12–16 month old transgenic mice or wildtype littermates from a colony set up using the APPswe/PS1dE9 strain (APP/PS1) (JAX), known to accumulate vascular and parenchymal Aβ deposits [13], and have been approved by the institutional Animal Ethics Committee (DEC) at the Leiden University Medical Center, permit number 09132. Besides standard genotyping, after each experiment amyloid pathology was confirmed by standard Thioflavin T staining.

Human material

Human brain tissue was obtained of AD/CAA patients or controls as confirmed by neuropathological examination in agreement with the guidelines of the ethics committee of the LUMC. Patient anonymity was strictly maintained. All tissue samples were handled in a coded fashion, according to Dutch national ethical guidelines (Code for Proper Secondary Use of Human Tissue, Dutch Federation of Medical Scientific Societies).

Murine specificity of the selected V_HH

To evaluate appropriate use of the APP/PS1 mouse model, murine cryosections (10 µm) were stained according previous protocols [9,12] with in addition a standard anti-mouse-to-mouse kit (ARK, Dako Cytomation). Final preparations were analyzed with an automated Pannoramic MIDI microscope (3DHistech).

Biodistribution and clearance

Radiolabeling. V_HH were labeled according to two different protocols. First, *his*-tagged V_HH were labeled directly with technetium-99m (^{99m}Tc) using a previously published protocol [14]. Briefly, 20 µl of V_HH in PBS solution (450–500 ng/µl) was added to 8 µl of an aseptic mixture of 950 mg/l $Sn(Cl)_2.2H_2O$ and 2 g/l $Na_4P_2O_7.10H_2O$ (Technescan PYP, Covidien, Petten, the Netherlands) in saline. After addition of 4 µl of 10 mg/ml of KBH_4 (crystalline, Sigma Chemical Co, St. Louis, MO) in 0.1 M NaOH, and 100 µl of $Na[^{99m}TcO_4]$ solution (approximately 200–700 MBq/ml, Technekow, Covidien, Petten, the Netherlands) the mixture was gently stirred at room temperature for at least 30 min before use. Analysis of the labeling solution, referred to as ^{99m}Tc-V_HH, yielded a radiochemical purity of >95% without detectable unreduced or free $^{99m}TcO_4$ [15].

Secondly, untagged V_HH were chelated for indium-111 (^{111}In) using diethylene triamine penta-acetic acid (DTPA). Untagged pa2H was chelated in a total volume of 1.0 ml with 20-fold molecular excess of *p*-SCN-Bn-DTPA (Macrocyclics, Dallas, TX) at pH 8.5 in phosphate buffer for 5 hr at 37.5°C and purified by dialysis using phosphate buffered saline (PBS). ^{111}In chloride (25 µl, 111 MBq/ml, Covidien, the Netherlands) was added to DTPA-pa2H conjugate (0.1 ml) in 0.25 M ammonium acetate buffer (0.8 ml) at pH 5.5 and incubated for 1 hr at room temperature. The reaction was quenched with 50 mM ethylene diamine tetra-acetic acid (EDTA) (50 µl) to chelate residual non-bound ^{111}In and the radiolabeled antibody was then purified using

Table 1. Biodistribution of ^{99m}Tc-ni3A in mice.

	t = 3 hr		t = 6 hr		t = 24 hr	
Tissue/organ	**Wildtypes**	**APP/PS1**	**Wildtypes**	**APP/PS1**	**Wildtypes**	**APP/PS1**
blood	1.202 ±0.379	1.146 ±0.131	0.778 ±0.048	0.808 ±0.115	0.451 ±0.073	0.363 ±0.051
heart	0.525 ±0.129	0.508 ±0.109	0.347 ±0.049	0.337 ±0.127	0.252 ±0.041	0.216 ±0.014
lungs	0.850 ±0.184	0.819 ±0.208	0.659 ±0.184	0.743 ±0.301	0.375 ±0.113	0.291 ±0.055
liver	1.078 ±0.235	1.000 ±0.293	1.078 ±0.188	1.223 ±0.424	0.568 ±0.149	0.488 ±0.164
kidneys	15.531 ±2.986	15.192 ±3.075	10.266 ±1.657	14.294 ±4.337	9.089 ±6.152	9.901 ±1.158
spleen	0.590 ±0.257	0.531 ±0.084	0.792 ±0.144	0.753 ±0.291	0.397 ±0.056	0.465 ±0.234
muscle	0.171 ±0.075	0.120 ±0.069	0.111 ±0.088	0.086 ±0.022	0.043 ±0.007	0.048 ±0.008
cerebrum	0.035 ±0.009	0.035 ±0.007	0.031 ±0.007	0.035 ±0.008	0.018 ±0.003	0.019 ±0.001
cerebellum	0.073 ±0.031	0.063 ±0.009	0.098 ±0.009	0.096 ±0.014	0.029 ±0.005	0.026 ±0.002
cerebrum/blood ratio	0.030 ±0.003	0.030 ±0.004	0.040 ±0.010	0.043 ±0.004	0.040 ±0.001	0.053 ±0.008*
cerebrum/muscle ratio	0.242 ±0.142	0.335 ±0.116	0.407 ±0.270	0.428 ±0.171	0.422 ±0.029	0.403 ±0.100

* = $P<0.05$ *wildtype mice compared to APP/PS1 mice.*

A bolus injection of 2 μg ^{99m}Tc-ni3A was administered intravenously into 12–14 month old APP/PS1 mice or their wild type littermates. At three time points after injection the animals were sacrificed and various tissues and entire organs were removed, weighed and counted for radioactivity. Values are expressed as a percentage of the injected dose per gram tissue (mean ± SD).

doi:10.1371/journal.pone.0038284.t001

a Sephadex^{TM} G-25 column (PD 10; GE Healthcare) eluted with PBS. Radiochemical purity assessed by instant thin layer chromatography (ITLC) yielded a purity of >95%.

Biodistribution and brain uptake. To study the biodistribution, animals were injected intravenously with 0.2 ml radiolabeled V_HH diluted with saline (5–10 MBq/ml, 10 μg/ml). At different intervals (t = 3–6–24 hrs) post-injection APP/PS1 (n = 4) and wildtype animals (n = 4) were sacrificed (Euthanasol, AST Pharma). Similar biodistribution experiments using untagged DTPA(^{111}In)-pa2H were only performed at 24 hours post-injection for APP/PS1 (n = 6) and wildtype mice (n = 6). Blood was collected via cardiac puncture, and various organs were removed, including the brain, which was divided into the cerebrum and cerebellum. All were weighed and counted for radioactivity (Wizard^2, Perkin Elmer). After decay correction, radioactivity was expressed as the percentage of the total injected dose of radioactivity per gram tissue (%ID/g). Blood/cerebrum ratios were calculated to correct for possible confounding effects accountable by residual blood. Similarly, muscle/cerebrum determined target-to-non-target ratios. Differences were regarded significant when $p \leq 0.05$ using an unpaired one or two tailed *t*-test. Experiments at t = 24 hrs were repeated twice using ^{99m}Tc-pa2H.

Blood clearance and analysis. Simultaneously, blood half-life was examined by collecting 5 μl tail samples at several time

Table 2. Biodistribution of radiolabeled pa2H in mice.

	^{99m}Tc-pa2H						DTPA(^{111}In)-pa2H	
	t = 3 hr		t = 6 hr		t = 24 hr		t = 24 hr	
Tissue/organ	**Wildtypes**	**APP/PS1**	**Wildtypes**	**APP/PS1**	**Wildtypes**	**APP/PS1**	**Wildtypes**	**APP/PS1**
blood	0.566 ±0.003	0.654 ±0.015	1.009 ±0.054	1.244 ±0.123	0.575 ±0.084	0.696 ±0.049	0.006 ±0.001	0.004 ±0.002
heart	0.273 ±0.121	0.240 ±0.017	0.623 ±0.101	0.763 ±0.031	0.367 ±0.059	0.393 ±0.007	0.017 ±0.084	0.014 ±0.003
lungs	0.843 ±0.256	0.537 ±0.010	0.930 ±0.242	1.088 ±0.035	0.620 ±0.160	0.622 ±0.031	0.016 ±0.011	0.014 ±0.003
liver	2.615 ±0.796	1.866 ±0.016	3.014 ±1.021	3.392 ±1.932	1.430 ±0.402	1.161 ±0.470	0.066 ±0.029	0.075 ±0.0.23
kidneys	9.243 ±1.787	6.241 ±0.530	14.306 ±4.105	15.612 ±1.042	9.824 ±2.810	8.608 ±0.738	8.859 ±3.623	7.689 ±2.930
spleen	1.515 ±0.503	1.319 ±0.060	6.498 ±1.623	6.258 ±0.208	3.584 ±1.381	1.747 ±0.100	0.044 ±0.022	0.048 ±0.006
muscle	0.356 ±0.379	0.054 ±0.006	0.174 ±0.022	0.347 ±0.026	0.102 ±0.023	0.113 ±0.018	0.059 ±0.020	0.059 ±0.044
cerebrum	0.014 ±0.003	0.017 ±0.001	0.033 ±0.005	0.044 ±0.004	0.027 ±0.004	0.038 ±0.002*	0.001 ±0.000	0.001 ±0.001
cerebellum	0.023 ±0.001	0.026 ±0.001	0.054 ±0.016	0.067 ±0.001	0.030 ±0.007	0.045 ±0.000*	0.003 ±0.001	0.002 ±0.001
cerebrum/blood ratio	0.025 ±0.005	0.026 ±0.003	0.033 ±0.004	0.035 ±0.004	0.047 ±0.003	0.055 ±0.008	0.013 ±0.011	0.041 ±0.055
cerebrum/muscle ratio	0.083 ±0.081	0.309 ±0.067	0.190 ±0.007	0.177 ±0.135	0.270 ±0.032	0.346 ±0.377	0.113 ±0.066	0.203 ±0.146

* = $P<0.05$ *wildtype mice compared to APP/PS1 mice.*

A bolus injection of 2 μg radiolabeled pa2H was administered intravenously into 12–14 month old APP/PS1 mice or their wildtype littermates. At three or one time points after injection of radiolabeled pa2H respectively with or without additional peptide tags, the animals were sacrificed and various tissues and entire organs were removed, weighed and counted for radioactivity. Values are expressed as a percentage of the injected dose per gram tissue (mean ± SD).

doi:10.1371/journal.pone.0038284.t002

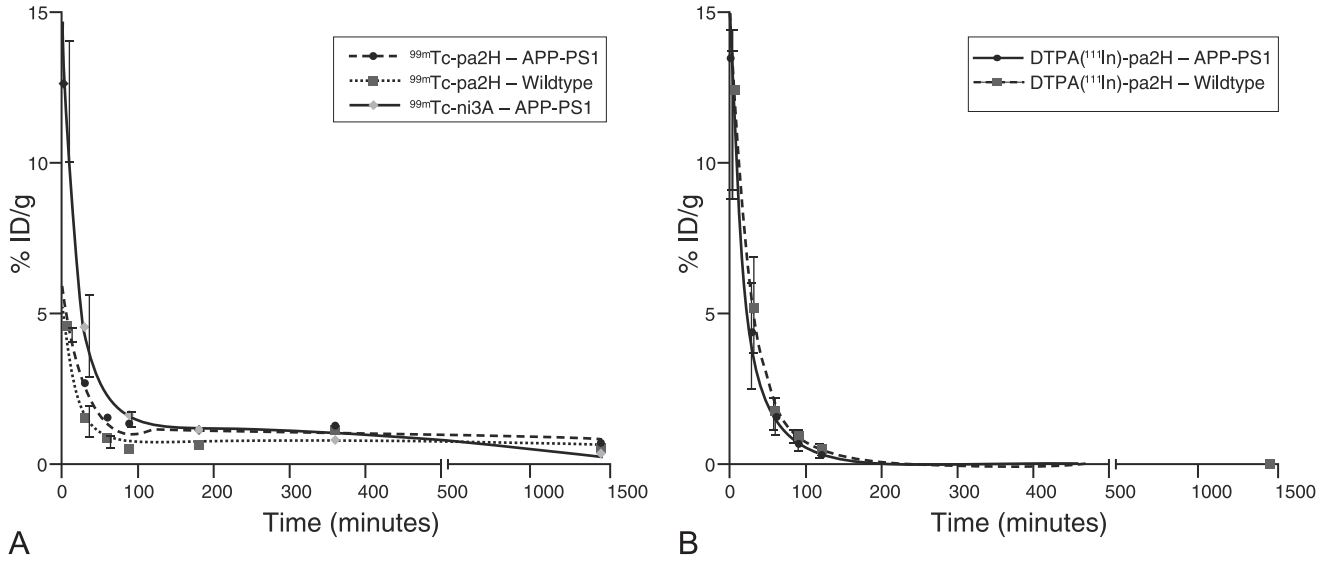

Figure 2. Blood clearance. These graphs represent the blood half lives of tagged ^{99m}Tc-ni3A and -pa2H (**A**), and untagged DTPA(^{111}In)-pa2H (**B**) in APP/PS1 mice and wildtype littermates. Data is shown as percentage of injected dose per gram of blood (%ID/g) over time. Based upon this plot the clearance is suggested to respectively consist of a fast and a slow phase, or only a single phase.
doi:10.1371/journal.pone.0038284.g002

points between 3–90 minutes post-injection of radiolabeled V_HH into transgenic or wildtype mice (n = 4–6). Combined with the cardiac blood samples corresponding half-lives were calculated using GraphPad Prism.

Similarly, 10 µl samples obtained at 10 and 90 minutes post-injection were mixed with 90 µl heparin (34 U/ml saline) and 900 µl PBS. Centrifugation for 10 minutes at 7,000 rpm separated plasma from the cell pellet. Radioactivity was measured separately to determine the blood distribution of radiolabeled V_HH over time.

Specificity of radiolabeled pa2H. Aβ specificity of pa2H-*his* after ^{99m}Tc-radiolabeling was tested by quantitative competition autoradiography. Human and murine brain cryosections (20 µm) were blocked with 1% bovine serum albumin (BSA)/PBS at 37°C for 1 hour followed by similar application of the labeling solution, which was diluted to 1 µg/ml by 1%BSA/PBS with or without additional 1 hour pre-incubation with excess monomeric or fibrillar $A\beta_{1-40}$ (rPeptide) at 37°C. Fibrils were produced using existing protocols [16].

After rinsing 3 times with PBS, radioactivity was counted for 15 minutes by a gamma camera (Toshiba GCA7100/UI). A similar region of interest was fitted for each scintigram to assess binding of ^{99m}Tc-pa2H-*his* with 0.1 ml of diluted labeling solution as a reference. Binding was expressed as the % of radioactivity compared to the section without any competitor. Experiments were performed in triplicate.

Table 3. Blood half lives of radiolabeled V_HH.

		Fast $t_{½}$			Slow $t_{½}$		
V_HH	**genotype**	*(min)*	*(95% C.I.)*	**%**	*(min)*	**%**	*(95% C.I.)*
^{99m}Tc-ni3A	APP/PS1	14.71	*(8.65–49.13)*	89.7	580	10.3	*(101.8–∞)*
	Wildtype	*ND*		*ND*	*ND*	*ND*	
^{99m}Tc-pa2H	APP/PS1	21.89	*(14.24–39.38)*	79.8	2562	20.2	*(975.0–∞)*
	Wildtype	10.78	*(7.27–20.76)*	87.1	5861	12.9	*(969.3–∞)*
DTPA(^{111}In)-pa2H	APP/PS1	19.69	*12.63–44.60*	100	-	-	
	Wildtype	15.83	*9.30–53.37*	100	-	-	

Half lives were determined by fitting a one or a two phase exponential decay model based on blood obtained from both tail vein and cardiac puncture at several time points after intravenous bolus injection of 2 µg radiolabeled V_HH in 12–14 month old APP/PS1 mice and wildtype littermates, as depicted in Figure 2. Please note that DTPA(^{111}In)-pa2H was produced without any additional peptide tags.
doi:10.1371/journal.pone.0038284.t003

In vivo Aβ targeting by V_HH

Fluorescent labeling. Tagged V_HH were fluorescently labeled with Alexa Fluor 594 protein labeling kit (Molecular Probes, Invitrogen) according to the manufacturer's guidelines, except using only half of the recommended amount of dye. Briefly spun to remove possible aggregates, extensive dialysis removed

Table 4. Blood distribution of ^{99m}Tc-pa2H.

Sample	**Time p.i.**	**Fraction**	**APP/PS1**		**Wildtype**	
	(min)		*(%)*	*sd*	*(%)*	*sd*
^{99m}Tc-pa2H	10	Plasma	88,9	6,2	80,3	5,2
		Cell Pellet	11,1		19,7	
	90	Plasma	83,6	8,7	72,0	8,2
		Cell Pellet	16,4		28,0	

At different time point after bolus injection of ^{99m}Tc-pa2H blood collected from the tail vein of 12–14 month old APP/PS1 mice or wildtype littermates. Separated into the cell pellet and plasma, samples were counted for radioactivity. Fractions are expressed in percentage of total activity at that time point. No significant differences were calculated using a student *t*-test ($p<0.05$).
doi:10.1371/journal.pone.0038284.t004

Table 5. Quantitative autoradiography.

Brain tissue	Binding of ^{99m}Tc-V_HH	Competion binding	
		Monomeric Aβ	Fibrillar Aβ
	ng (± sd)	ng (± sd)	ng (± sd)
APP/PS1	98.8 (±20,7)*	60.1 (±22.2)	31.4 (±14.3)
Wildtype	86.4 (±14.8)	56.4 (±19.5)	27.1 (±12.5)
AD human	190.1 (±73.5)*	81.4 (± N.D.)	42.3 (±29.2)
Control human	102.3 (±30.2)	27.2 (± N.D.)	49.9 (±17.4)

Differences in radioactivity were measured after application of 1 μg ^{99m}Tc-pa2H to human and murine APP/PS1 brain sections.
*Statistical difference ($p<0.05$) between either murine or human control versus Aβ bearing sections.
doi:10.1371/journal.pone.0038284.t005

excess free label. The labeling degree and protein concentration (200–600 ng/μl) were determined using the Nanodrop ND1000 (Isogen Life Sciences). Protein integrity was confirmed by mass spectrometry.

Immunofluorescence using VHH-Alexa594. To examine whether the fluorescent labeling affected antigen recognition, human and murine cryosections (10 μm) were rinsed with PBS, fixed in ice-cold acetone for 10 minutes before overnight incubation with V_HH- Alexa594 in 1% BSA/PBS in a wet chamber. Washed 3×5 minutes with PBS, sections were mounted and analyzed using a fluorescence microscope (Leica DMR5500B).

In vivo Aβ imaging by topical application. Four APP/PS1 animals received permanent cranial windows to allow serial *in vivo* imaging of the brain by multiphoton microscopy. Animals were anaesthetized using 2% isoflurane gas inhalation, and the exposed skull was partly replaced by a round glass coverslip glued into place using Krazyglue® according to previous surgical protocols [17,18]. Prior to fixation of the cranial window, a drop of 40–60 μl of V_HH-Alexa594 (275–400 ng/μl) was applied directly onto the exposed brain for 30 minutes and briefly rinsed with PBS. Colocalization with the Aβ deposits was based either upon their typical green autofluorescence or by intraperitoneal injections of Methoxy-X04 one day prior surgery [16]. Animals were imaged immediately following surgery, which was typically less than 90 minutes after beginning of the procedure, and re-imaged under isoflurane anaethesia (2%) for several days to study the washout. Images were acquired with a Bio-Rad 1024 multiphoton microscope equipped with a Ti:Sapphire laser (Mai Tai, Spectra Physics) and external photodetectors (Hamamatsu Photonics). Areas were imaged to approximately 200 μm deep in 5 μm steps with a 20× objective (UMPlanFl, NA = 0.95; Olympus). Maximum intensity projections were reconstructed using ImageJ.

Specific in vivo Aβ binding after BBB disruption. A systemic approach to study the in vivo behaviour of the VHH throughout a larger area within the brain involved intracarotid infusion (60 μl/min) of 100 μl pa2H-his-Alexa594 along with 600 μl 15% mannitol selectively into the right carotic artery to disrupt the BBB [19]. At t = 2 and 24 hours post-injection., transgenic (n = 9) and wildtype animals (n = 3) were euthanized (Euthanasol, AST Pharma), and perfused with 4% paraformaldehyde (PFA). Resected brains were stored in 4% PFA with 10% sucrose for 4 hours followed by overnight fixation in 4% PFA with 30% sucrose. Next, the brains were snap frozen and sectioned completely to obtain consecutive 30-μm-thick cryosections. Besides standard Thioflavin T staining for amyloid, adjacent sections were immunostained for Aβ (6F/3D, DakoCytomation) [20] with 1:100 goat-antimouse-Alexa488 (Invitrogen) to assess colocalization. Images obtained by a Leica DM5500B microscope were merged using Adobe Photoshop CS3.

Results

Murine specificity of the selected V_HH

Immunostained brain sections of aged APP/PS1 and wildtype littermates using tagged V_HH ni3A and pa2H were made to assess their capacity to selectively recognize different types of deposits. (Figure 1) Pa2H stained positive for all forms of Aβ depositions. In this transgenic mouse model, ni3A did not show selective affinity for vascular Aβ; both vascular and parenchymal Aβ depositions were clearly labeled. Compared to ni3A, equivalent staining protocols with pa2H resulted in higher specificity for Aβ combined with a low unspecific background binding. For neither V_HH specific affinity was detected within the brain sections of wildtype animals.

Biodistribution and clearance

Biodistribution and brain uptake. The distribution of a bolus injection of radiolabeled tagged ni3A and pa2H over time is shown in Table 1 and 2. No significant differences in organ uptake between wildtype and transgenic animals were found, except for the brain uptake of ^{99m}Tc-pa2H after 24 hours. Although the amount was low (0.038%I.D./g), cerebral uptake was 40% higher in the transgenic animals. The cerebrum/blood ratio did not differ, indicating that this difference was not caused by different V_HH concentrations within the blood pool. For the cerebellum similar results were found. Repeated experiments for this particular endpoint resulted in similar findings.

To investigate whether these findings were not confounded by either the non-specific radiolabeling procedure or the presence of additional peptide tags, the biodistribution experiment was repeated with untagged DTPA(^{111}In)-pa2H. (Table 2) With this labeling protocol, we no longer observed a significantly higher cerebral uptake in amyloid-bearing mice. Regardless of the tag, the majority of radiolabeled V_HH was excreted via the kidneys. Cellular involvement as shown by distinctive hepatic clearance or splenal activity was low. In comparison to ^{99m}Tc-ni3A, ^{99m}Tc-pa2H showed about 3 times higher clearance via liver and spleen. Also, the clearance rate for ^{99m}Tc-pa2H was lower, independent of genotype. However, within the first 3 hours ^{99m}Tc-ni3A resulted in a higher general organ uptake, with exception of the aforementioned liver and spleen.

Blood clearance and analysis. Blood clearance of the tagged ^{99m}Tc-V_HH consisted of a fast and a slow component. (Figure 2A) In general, the majority of the radiolabeled V_HH was cleared from the blood with a half-life of 10–20 minutes (Table 3). The actual half-life of the slow component of ^{99m}Tc- V_HH could only be calculated with limited accuracy, since the half-life was longer than the blood sampling period. In line with the above biodistribution, six hours post-injection, the blood levels of ^{99m}Tc-pa2H were remarkably higher compared to earlier time points, which is characteristic for a second passage. Within the first 90 minutes about 80% of the ^{99m}Tc-V_HH remained within the blood plasma, indicating that no significant cellular uptake occurred. (Table 4)

In contrast to tagged ^{99m}Tc- V_HH, the blood clearance of untagged DTPA(^{111}In)-pa2H was mono-exponential, with a similar rapid clearance within 20 minutes, but without a slow component. (Figure 2B)

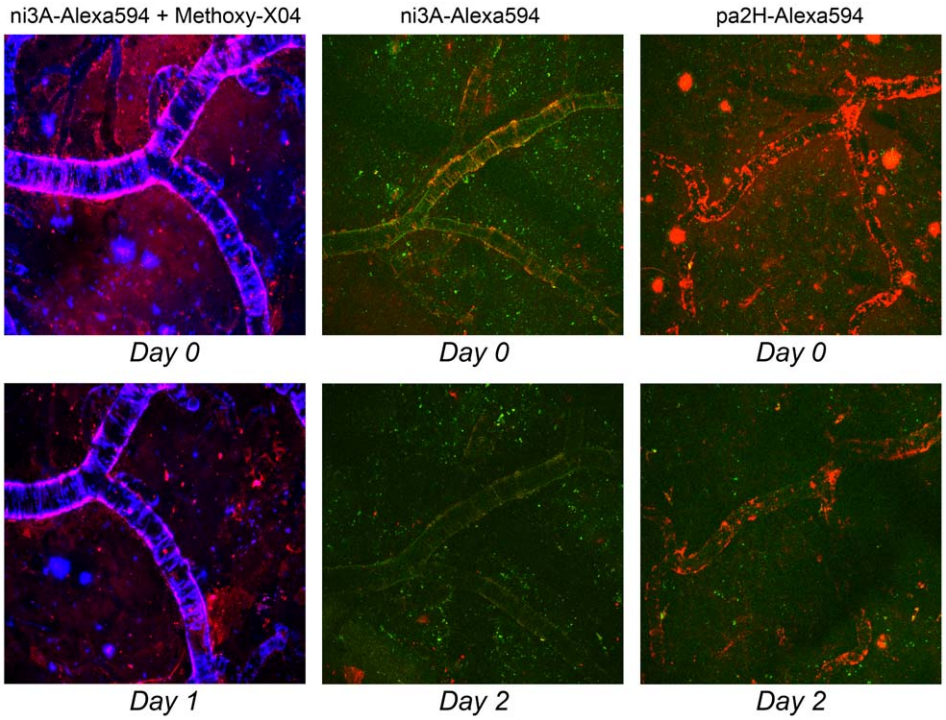

Figure 3. *In vivo* Aβ imaging after direct brain application. Topical application of ni3A- or pa2H-Alexa594 (*red*) as visualized over time by intravital multiphoton microscopy in APP/PS1 mice clearly shows the specific *in vivo* labeling of different Aβ deposits. In the ***left***, vascular and parenchymal Aβ deposits, detected by prior labeling with Methoxy-X04 (blue), colocalize with ni3A-Alexa594 (red) directly following topical application. One day later, labeling of the plaques has diminished to almost none with some residual left bound to CAA. With interpretation hampered by Methoxy-X04, ***middle*** images show a similar experiment. Colocalization with Aβ deposits based upon autofluorescence (*green*) gave comparable results and almost complete wash out after two days. Pa2H-Alexa594 (red), as shown in the ***right*** images, remains bound to vascular Aβ even two days after application, when the plaques remained undetected. All images are maximum intensity projections of a 3D cortical volume with a field of view 615×615 μm.
doi:10.1371/journal.pone.0038284.g003

Specificity of 99mTc-pa2H. After radiolabeling of the tagged pa2H it's specificity for Aβ was unaffected, as shown by scintigraphic analysis; binding of ^{99m}Tc-pa2H was higher in those sections including Aβ. (Table 5) Furthermore, binding was significantly ($p<0.001$) reduced when the tracer was pre-incubated with either monomeric or fibrillar Aβ.

In vivo Aβ targeting by V_HH

In vivo Aβ imaging by topical application. After direct application onto the exposed mouse brain, fluorescent V_HH were followed up for at least 48 hours by *in vivo* multiphoton microscopy. (Figure 3) Specific *in vivo* labeling of Aβ plaques by ni3A-Alexa594 was initially confirmed by colocalization with Methoxy-X04, a known *in vivo* amyloid targeting fluorophore. Beside possible binding competition with the V_HH, Methoxy-X04 hampered good validation due to signal cross-over into the red channel. However, colocalization based on the typical autofluorescence patterns of the different Aβ deposits resulted in similar findings. Selectivity was confirmed by lack of nonspecific background signal. Although both V_HH were capable of targeting Aβ *in vivo*, only pa2H-Alexa594 was detectable after two days, mainly bound to vascular amyloid.

Specific in vivo Aβ binding after BBB disruption. Based on the above findings, co-injections of pa2H-Alexa594 with mannitol were done in the right carotid artery to selectively open the BBB in the ipsilateral hemisphere to study the in vivo characteristics throughout the brain. Two hours post-injection, fluorescence was detected in the right hemisphere, co-localizing with Aβ. (Figure 4) Even within the deeper brain structures, no nonspecific binding was observed. Aβ related fluorescent signal remained detectable for at least 24 hours post-injection. Without BBB disruption or within wildtype littermates, no apparent Aβ labeling could be detected.

Immunofluorescence using VHH-Alexa594. Selectivity for specific Aβ deposits was not altered after fluorescent labeling of the VHH, since on human sections, ni3A-Alexa594 selectively stained vascular Aβ (Figure 5 A–C), and pa2H-Alexa594 stained both parenchymal and vascular Aβ.(Figure 5 G–I) On murine material all Aβ deposits were stained by both fluorescent VHH.(Figure 5 D–F & J–L)

Discussion

In this study, we assessed two previously described V_HH for their potential to cross the blood-brain barrier and distinctively detect vascular and parenchymal Aβ deposits *in vivo*.

Specific detection of parenchymal and vascular amyloid in APP/PS1 mice

Both V_HH stained positive for Aβ upon APP/PS1 brain sections confirming appropriate use of this transgenic model. *In vivo* binding to parenchymal and vascular Aβ was confirmed when the BBB was circumvented. Signal remained detectable for at least 24 hours while *in vivo* pa2H showed a high affinity combined with a low off-rate. However, previously shown selectivity for solely vascular Aβ in human post-mortem brain sections by ni3A was not

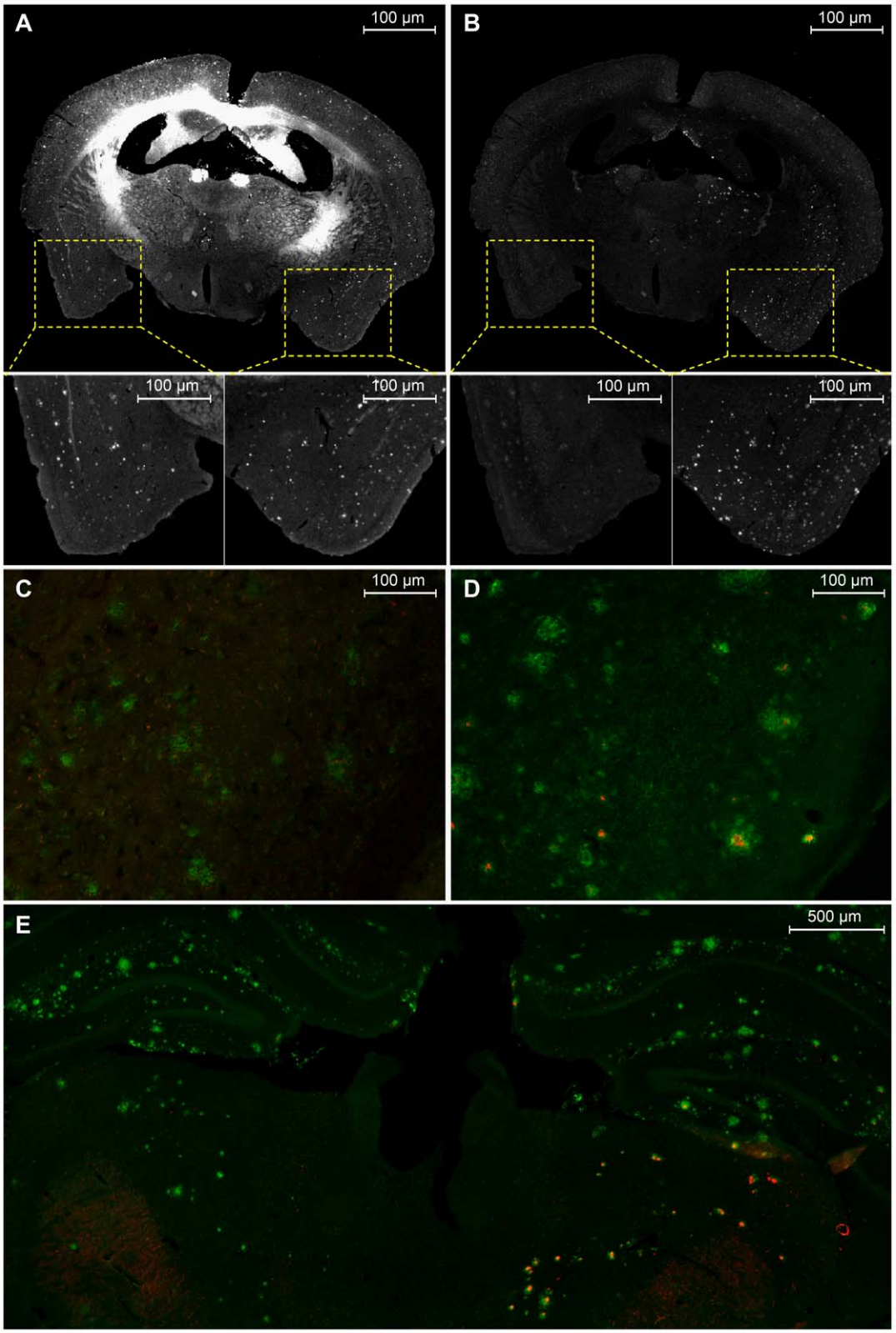

Figure 4. Specific *in vivo* Aβ binding after BBB disruption. After disruption of the BBB using a co-injection of 15% mannitol with pa2H-Alexa594 into the right carotid artery of an aged APP/PS1 mouse sacrificed 2 hrs post injection, amyloid plaques are clearly depicted in both hemispheres using a Thioflavin T (ThT) staining (**A**), while the pa2H-Alexa594 signal is only detected in the right hemisphere (**B**). More careful examination shows all Alexa594 signal colocalizes with ThT in the right hemisphere, while in the left only some autofluorescense can be detected. Furthermore, immunofluorescense anti-Aβ staining of the plaques using Alexa488 within the left hemisphere (**C**) results only in green signal, while within the right hemisphere (**D**) the red signal from pa2H-Alexa594 nicely colocalizes within the plaques. Experiments performed in a similar setting

but sacrificed 24 hrs post-injection, showed similar results with pa2H-Alexa594 still nicely corresponding to the green labeling of the anti-Aβ staining within the right hemisphere (**E**).
doi:10.1371/journal.pone.0038284.g004

observed within this mouse model (Figures 1,3,5). Fluorescent or radiolabeling prior *in vivo* application did not affect their specificity. The unique specific reactivity of ni3A for vascular amyloid deposition on human brain material is not yet completely understood [9]. Known differences in morphology and composition of human and murine Aβ deposits might help to understand ni3A's specific reactivity [21,22]. Human plaques consist of discontinuous patches with decreased density and random fibrillar orientation within the amyloid core; murine plaques are generally built up by long organized fibrils, resulting in densely packed amyloid plaques with a relatively large core [23]. Besides morphological differences, posttranslational modifications of Aβ differ from mouse to man leading to alterations of the Aβ molecule itself [21,24,25]. Differences in metal ion content are known to influence the tertiary structure [26,27]. Previous epitope mapping revealed that ni3A has no other cross reaction but to $A\beta_{1-42}$ [9], which is highly abundant in parenchymal and vascular deposits in both humans and APP/PS1 mice. All together, this leads to the conclusion that the selective reactivity of ni3A must depend on the structural presentation of $A\beta_{1-42}$, in which case murine parenchymal plaques probably show structural similarities to human CAA.

In vivo blood-brain barrier passage

Previous *in vitro* data suggested that our V_HH actively migrated across the BBB in a more efficient way than FC5, a V_HH specifically selected to pass the BBB [12]. However, the *in vivo* experiments resulted only in a small cerebral uptake of the tagged ^{99m}Tc-pa2H at 24 hours after intravenous administration, and the current brain uptake levels were insufficient to assess the uptake kinetics *in vivo* with for example SPECT imaging. (data not shown) Additional experiments with untagged DTPA(^{111}In)-pa2H further confirmed the current limitations as hardly any cerebral uptake was observed with this labeling protocol. The increased brain uptake for 99mTc-pa2H compared to DTPA(^{111}In)-pa2H may be due to the slower blood clearance for ^{99m}Tc-pa2H. The observed fast blood clearance and relatively high renal retention for the VHH in this study is in line with previous reports [28,29], and

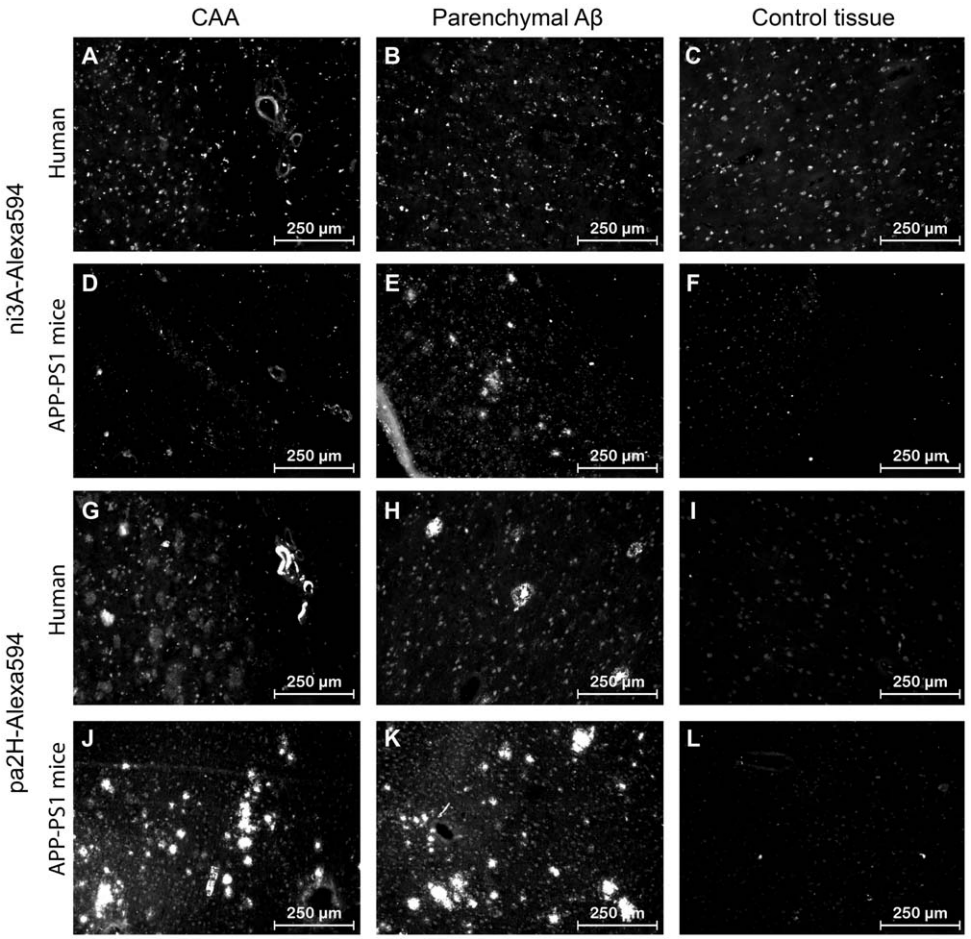

Figure 5. Immunofluorescence with V_HH-Alexa594. Shown are the results of immunofluorescence staining with ni3A- and pa2H-Alexa594 on cryosections of APP/PS1 murine and human AD/CAA brain tissue, including wildtype or healthy controls. Both V_HH stain positive for CAA in all sections (**A**, **D**, **G**, **J**). Only ni3A-Alexa594 stained negative for human parenchymal Aβ (**B**), while pa2H stained positive for several types of parenchymal Aβ deposits (**G**, **H**, **J**, **K**) in both humans and mice. In either human of murine control tissue no such staining patterns were observed.(**C**, **F**, **I**, **L**)
doi:10.1371/journal.pone.0038284.g005

typical for peptides and proteins smaller than the filtering threshold of the glomerular membrane (<60 kDa) [30]. However, in general, a short blood residential time effectively reduces the blood-to-brain transfer.

In vivo studies with the BBB crossing V_HH FC5 demonstrated 4%ID/g brain uptake, which is much higher than our findings [31]. This discrepancy may be due to the lower dose that we used, but several other factors may also play a part. For FC5 it is known it uses receptor-mediated endocytosis via the α(2,3)-sialoglycoprotein [32]. For our V_HH, *in vitro* active transport mechanisms are involved, but the specific receptors are as yet unknown [12]. Possibly, the *in vivo* BBB passage may be limited by the availability of these receptors in our mouse model.

To improve BBB penetration for the amyloid-targeting V_HH, one could increase the blood circulation time by multimerization or by conjugating the V_HH to an albumin-targeting moiety or V_HH [33,34]. An alternative approach would be to incorporate the V_HH into a BBB-targeting nanoparticle. Recently, several nanoparticle carrier systems have been developed for brain delivery of therapeutics that would also be suitable for loading with V_HH [35].

Diagnostic and therapeutic value of V_HH

In general, V_HH constitute many unique characteristics that make them interesting tools for either diagnostics or therapeutics. Compared to conventional monoclonal antibodies or Fab', V_HH express a similar unique level of specificity and affinity, but because of their single domain, production and modification is relatively easy and cost-efficient [29].

Currently used amyloid-targeting ligands, like ^{11}C-PiB recognize amyloid plaques rather than Aβ. In contrast, we already showed that V_HH may be more specific to a certain sub-types of Aβ accumulation [9]. Further selection may allow the *in vivo* detection of the full range of Aβ aggregates from oligomers to dense core plaques to CAA.

Besides diagnostics, several V_HH have shown their potential therapeutic value in vitro, preventing aggregation of amyloid fibrils, oligomeric forms of Aβ and polyA-binding protein nuclear 1 [36–39]. In the latter case, even complete clearance of existing aggregates was reported. Whether V_HH evaluated in this study possess similar abilities is currently under investigation. However, within the data presented here, we observed that several Aβ plaques, as detected by their autofluorescence, could no longer be seen two days after V_HH application. (Figure 3) Whereas current passive immunotherapies targeting Aβ are hampered by unwanted immunogenic side effects, repetitive administration of V_HH has shown to be non-immunogenic [4,40]. Furthermore, their selective binding to different Aβ species, like ni3A's specific binding for CAA, could shift Aβ brain efflux in the favored direction, which could be used to tailor anti-Aβ therapy to further reduce therapy-induced complications, e.g. CAA related microbleeds [4,5,41].

These initial *in vivo* studies to investigate whether Aβ specific V_HH can be exploited as diagnostic tools show promising results for further development. Although capable of strong specific binding *in vivo* with low unspecific background binding and favorable wash-out, issues regarding higher brain uptake and clearance need to be addressed in the future.

Author Contributions

Conceived and designed the experiments: RN KR MW BB MvB SM LW. Performed the experiments: RN KR MW AM MdB MR. Analyzed the data: RN KR MW AM MdB MR BB MvB SM LW. Contributed reagents/materials/analysis tools: RN KR MW AM MdB BB. Wrote the paper: RN KR MW BB MvB SM LW.

References

1. Duyckaerts C, Delatour B, Potier MC (2009) Classification and basic pathology of Alzheimer disease. Acta Neuropathol 118: 5–36. doi:10.1007/s00401-009-0532-1.
2. Smith EE, Greenberg SM (2009) Beta-amyloid, blood vessels, and brain function. Stroke 40: 2601–2606. doi:10.1161/STROKEAHA.108.536839.
3. Weller RO, Preston SD, Subash M, Carare RO (2009) Cerebral amyloid angiopathy in the aetiology and immunotherapy of Alzheimer disease. Alzheimers Res Ther 1: 6. doi:10.1186/alzrt6.
4. Jicha GA (2009) Is passive immunization for Alzheimer's disease 'alive and well' or 'dead and buried'? Expert Opin Biol Ther 9: 481–491. doi:10.1517/14712590902828285.
5. Greenberg SM, Bacskai BJ, Hyman BT (2003) Alzheimer disease's double-edged vaccine. Nat Med 9: 389–390. doi:10.1038/nm847.
6. Jack CR Jr., Knopman DS, Jagust WJ, Shaw LM, Aisen PS, et al. (2010) Hypothetical model of dynamic biomarkers of the Alzheimer's pathological cascade. Lancet Neurol 9: 119–128. doi:10.1016/S1474-4422(09)70299-6.
7. Frisoni GB, Fox NC, Jack CR Jr., Scheltens P, Thompson PM (2010) The clinical use of structural MRI in Alzheimer disease. Nat Rev Neurol 6: 67–77. doi:10.1038/nrneurol.2009.215.
8. Johnson KA, Gregas M, Becker JA, Kinnecom C, Salat DH, et al. (2007) Imaging of amyloid burden and distribution in cerebral amyloid angiopathy. Ann Neurol 62: 229–234. doi:10.1002/ana.21164.
9. Rutgers KS, van Remoortere A, van Buchem MA, Verrips CT, Greenberg SM, et al. (2009) Differential recognition of vascular and parenchymal beta amyloid deposition. Neurobiol Aging doi:10.1016/j.neurobiolaging.2009.11.012.
10. Hamers-Casterman C, Atarhouch T, Muyldermans S, Robinson G, Hamers C, et al. (1993) Naturally occurring antibodies devoid of light chains. Nature 363: 446–448. doi:10.1038/363446a0.
11. Harmsen MM, De Haard HJ (2007) Properties, production, and applications of camelid single-domain antibody fragments. Appl Microbiol Biotechnol 77: 13–22. doi:10.1007/s00253-007-1142-2.
12. Rutgers KS, Nabuurs RJ, van den Berg SA, Schenk GJ, Rotman M, et al. (2011) Transmigration of beta amyloid specific heavy chain antibody fragments across the in vitro blood-brain barrier. Neuroscience doi:10.1016/j.neuroscience.2011.05.076.
13. Jankowsky JL, Slunt HH, Ratovitski T, Jenkins NA, Copeland NG, et al. (2001) Co-expression of multiple transgenes in mouse CNS: a comparison of strategies. Biomol Eng 17: 157–165.
14. Welling MM, Paulusma-Annema A, Balter HS, Pauwels EK, Nibbering PH (2000) Technetium-99m labelled antimicrobial peptides discriminate between bacterial infections and sterile inflammations. Eur J Nucl Med 27: 292–301.
15. Welling MM, Korsak A, Gorska B, Oliver P, Mikolajczak R, et al. (2005) Kit with technetium-99m labelled antimicrobial peptide UBI 29–41 for specific infection detection. Journal of Labelled Compounds & Radiopharmaceuticals 48: 683–691. doi:10.1002/jlcr.961.
16. Klunk WE, Bacskai BJ, Mathis CA, Kajdasz ST, McLellan ME, et al. (2002) Imaging Abeta plaques in living transgenic mice with multiphoton microscopy and methoxy-X04, a systemically administered Congo red derivative. J Neuropathol Exp Neurol 61: 797–805.
17. Skoch J, Dunn A, Hyman BT, Bacskai BJ (2005) Development of an optical approach for noninvasive imaging of Alzheimer's disease pathology. J Biomed Opt 10: 11007. doi:10.1117/1.1846075.
18. Robbins EM, Betensky RA, Domnitz SB, Purcell SM, Garcia-Alloza M, et al. (2006) Kinetics of cerebral amyloid angiopathy progression in a transgenic mouse model of Alzheimer disease. J Neurosci 26: 365–371. doi:10.1523/JNEUROSCI.3854-05.2006.
19. Wadghiri YZ, Sigurdsson EM, Wisniewski T, Turnbull DH (2005) Magnetic resonance imaging of amyloid plaques in transgenic mice. Methods Mol Biol 299: 365–379.
20. Natte R, Maat-Schieman ML, Haan J, Bornebroek M, Roos RA, et al. (2001) Dementia in hereditary cerebral hemorrhage with amyloidosis-Dutch type is associated with cerebral amyloid angiopathy but is independent of plaques and neurofibrillary tangles. Ann Neurol 50: 765–772.
21. Duyckaerts C, Potier MC, Delatour B (2008) Alzheimer disease models and human neuropathology: similarities and differences. Acta Neuropathol 115: 5–38. doi:10.1007/s00401-007-0312-8.
22. Guntert A, Dobeli H, Bohrmann B (2006) High sensitivity analysis of amyloid-beta peptide composition in amyloid deposits from human and PS2APP mouse brain. Neuroscience 143: 461–475. doi:10.1016/j.neuroscience.2006.08.027.
23. van Groen T, Kiliaan AJ, Kadish I (2006) Deposition of mouse amyloid beta in human APP/PS1 double and single AD model transgenic mice. Neurobiol Dis 23: 653–662. doi:10.1016/j.nbd.2006.05.010.
24. Bussiere T, Bard F, Barbour R, Grajeda H, Guido T, et al. (2004) Morphological characterization of Thioflavin-S-positive amyloid plaques in transgenic Alzheimer mice and effect of passive Abeta immunotherapy on their clearance. Am J Pathol 165: 987–995.

25. Richardson JA, Burns DK (2002) Mouse models of Alzheimer's disease: a quest for plaques and tangles. ILAR J 43: 89–99.
26. Adlard PA, Bush AI (2006) Metals and Alzheimer's disease. J Alzheimers Dis 10: 145–163.
27. Leskovjan AC, Lanzirotti A, Miller LM (2009) Amyloid plaques in PSAPP mice bind less metal than plaques in human Alzheimer's disease. Neuroimage 47: 1215–1220. doi:10.1016/j.neuroimage.2009.05.063.
28. Gainkam LO, Huang L, Caveliers V, Keyaerts M, Hernot S, et al. (2008) Comparison of the biodistribution and tumor targeting of two 99mTc-labeled anti-EGFR nanobodies in mice, using pinhole SPECT/micro-CT. J Nucl Med 49: 788–795. doi:10.2967/jnumed.107.048538.
29. Huang L, Muyldermans S, Saerens D (2010) Nanobodies(R): proficient tools in diagnostics. Expert Rev Mol Diagn 10: 777–785. doi:10.1586/erm.10.62.
30. Behr TM, Goldenberg DM, Becker W (1998) Reducing the renal uptake of radiolabeled antibody fragments and peptides for diagnosis and therapy: present status, future prospects and limitations. Eur J Nucl Med 25: 201–212.
31. Muruganandam A, Tanha J, Narang S, Stanimirovic D (2002) Selection of phage-displayed llama single-domain antibodies that transmigrate across human blood-brain barrier endothelium. FASEB J 16: 240–242. doi:10.1096/fj.01-0343fje.
32. Abulrob A, Sprong H, Van Bergen en HP, Stanimirovic D (2005) The blood-brain barrier transmigrating single domain antibody: mechanisms of transport and antigenic epitopes in human brain endothelial cells. J Neurochem 95: 1201–1214. doi:10.1111/j.1471-4159.2005.03463.x.
33. Coppieters K, Dreier T, Silence K, de Haard H, Lauwereys M, et al. (2006) Formatted anti-tumor necrosis factor alpha VHH proteins derived from camelids show superior potency and targeting to inflamed joints in a murine model of collagen-induced arthritis. Arthritis Rheum 54: 1856–1866. doi:10.1002/art.21827.
34. Tijink BM, Laeremans T, Budde M, Stigter-van WM, Dreier T, et al. (2008) Improved tumor targeting of anti-epidermal growth factor receptor Nanobodies through albumin binding: taking advantage of modular Nanobody technology. Mol Cancer Ther 7: 2288–2297. doi:10.1158/1535-7163.MCT-07-2384.
35. Koffie RM, Farrar CT, Saidi LJ, William CM, Hyman BT, et al. (2011) Nanoparticles enhance brain delivery of blood-brain barrier-impermeable probes for in vivo optical and magnetic resonance imaging. Proc Natl Acad Sci U S A 108: 18837–18842. doi:10.1073/pnas.1111405108.
36. Chartier A, Raz V, Sterrenburg E, Verrips CT, van der Maarel SM, et al. (2009) Prevention of oculopharyngeal muscular dystrophy by muscular expression of Llama single-chain intrabodies in vivo. Hum Mol Genet 18: 1849–1859. doi:10.1093/hmg/ddp101.
37. Dumoulin M, Last AM, Desmyter A, Decanniere K, Canet D, et al. (2003) A camelid antibody fragment inhibits the formation of amyloid fibrils by human lysozyme. Nature 424: 783–788. doi:10.1038/nature01870.
38. Lafaye P, Achour I, England P, Duyckaerts C, Rougeon F (2009) Single-domain antibodies recognize selectively small oligomeric forms of amyloid beta, prevent Abeta-induced neurotoxicity and inhibit fibril formation. Mol Immunol 46: 695–704. doi:10.1016/j.molimm.2008.09.008.
39. Verheesen P, de Kluiver A, van Koningsbruggen S, de Brij M, De Haard HJ, et al. (2006) Prevention of oculopharyngeal muscular dystrophy-associated aggregation of nuclear polyA-binding protein with a single-domain intracellular antibody. Hum Mol Genet 15: 105–111. doi:10.1093/hmg/ddi432.
40. Stijlemans B, Conrath K, Cortez-Retamozo V, van Xong H, Wyns L, et al. (2004) Efficient targeting of conserved cryptic epitopes of infectious agents by single domain antibodies. African trypanosomes as paradigm. J Biol Chem 279: 1256–1261. doi:10.1074/jbc.M307341200.
41. Klunk WE, Lopresti BJ, Ikonomovic MD, Lefterov IM, Koldamova RP, et al. (2005) Binding of the positron emission tomography tracer Pittsburgh compound-B reflects the amount of amyloid-beta in Alzheimer's disease brain but not in transgenic mouse brain. J Neurosci 25: 10598–10606. doi:10.1523/JNEUROSCI.2990-05.2005.